Hindawi
Journal of Nanotechnology
Volume 2019, Article ID 4571848, 11 pages
https://doi.org/10.1155/2019/4571848

Research Article

Fe-TiO_2 Nanoparticles Synthesized by Green Chemistry for Potential Application in Waste Water Photocatalytic Treatment

Ricardo A. Solano,[1] **Adriana P. Herrera**,[1] **David Maestre**,[2] **and Ana Cremades**[2]

[1]*School of Engineering, Nanomaterials and Computer Aided Process Engineering Research Group, University of Cartagena, 130015 Cartagena, Colombia*
[2]*School of Physical Sciences, Department of Materials Physics, Universidad Complutense de Madrid, 28040 Madrid, Spain*

Correspondence should be addressed to Adriana P. Herrera; aherrerab2@unicartagena.edu.co

Received 2 August 2018; Revised 1 December 2018; Accepted 5 December 2018; Published 20 January 2019

Academic Editor: Marco Rossi

Anatase TiO_2 nanoparticles doped with iron ions have been synthesized via the green chemistry method using aqueous extract of lemongrass (*Cymbopogon citratus*) obtained from Soxhlet extraction and doped by wet impregnation. The TiO_2 anatase phase has been doped with Fe^{3+} (0.05, 0.075, and 0.1 Fe^{3+} : Ti molar ratio) at 550°C and 350°C, respectively. The scanning electron microscopy with energy-dispersive X-ray (SEM-EDS) shows nanoparticle clusters and efficiencies of impregnations between 66.5 and 58.4% depending on the theoretical dopant amount. The electron transmission microscopy (TEM) reveals final particle sizes ranging between 7 and 26 nm depending on the presence or not of the dopant. The cathodoluminescence (CL) and photoluminescence (PL) studies of the doped and undoped nanoparticles show a luminescence signal attributed to surface oxygen vacancies (visible CL emission 380–700 nm and PL emission 350–800 nm); additionally, a decrease in emission intensity is observed due the inhibition of the recombination of the photogenerated electron-holes pairs; moreover, nanopowders were analyzed by UV-Vis spectrophotometry of diffuse reflectance, and the absorption edge of the Fe-TiO_2 in comparison to undoped TiO_2 is extended greatly toward the visible light. The six bands (A_{1g} + $2B_{1g}$ + $3E_g$) found by Raman spectroscopy and the x-ray diffraction pattern (XRD) confirm that synthesized TiO_2 is only anatase phase, which is commonly used as a catalyst in waste water treatment, specifically in heterogeneous photocatalytic processes.

1. Introduction

Solar energy is a renewable resource, and its efficient utilization in controlling environmental pollutions by using photocatalytic materials is one of the main goals of modern science and engineering [1–4]. Owing to exceptional and appropriate properties including nontoxic, excellent chemical stability, strong ultraviolet (UV) absorption, and wide band gap energy (anatase 3.2 eV and rutile 3.4 eV), titanium dioxide (TiO_2) is a recognized metal oxide semiconductor which could be extensively applied to diverse applications. Hence, the utilization of sustainable luminous energy like visible light or sunlight is limited, because TiO_2 can only be excited by ultraviolet light (wavelength lower than 387 nm), which occupies only 3–5% of the entire solar spectrum [5–11]. It is also known that high recombination of activated electron-hole pair of TiO_2 is still its major drawback that causes the restriction of practical applications, in particular, solar harvesting aspect [10, 12, 13]. Thus, many approaches have been devoted to improve the light response of TiO_2 in the visible light region. For instance, nonmetal doping (B, C, N, S, and F), metal doping (Fe, Co, and La), and codoping (Fe and N, B and C) [14–25].

There are current research studies focusing on the use of plant extracts for the green synthesis of different types of nanomaterials because the phytochemicals present in these natural extracts participate as capping agents or templates for the stabilization of crystalline phases and size control of the nanoparticles produced [26–32]. Recently, a mixture of rutile with impurities for anatase phase has been prepared via green synthesis using *M. citrifolia* leaves extract by the hydrothermal method with calcination temperature 400°C.

The green synthesized compound has a tetragonal structure when characterized by XRD, and the evaluated average crystalline size was 10 nm; also, the surface morphology of TiO_2 nanoparticles obtained via green synthesis was observed as high uniform quasi-spherical shape morphology [33]. Furthermore, Rajiv et al. [34] biosynthesized TiO_2 nanoparticles (NPs) using the *Momordica charantia* leaf aqueous extract as a reducing and stabilizing agent, and these nanoparticles were applied in the *in vitro* antimalarial activity against *Plasmodium falciparum*, and the results suggest that the synthesized TiO_2 NPs may be employed to develop newer and safer agents for malaria control. In a similar study, Goutam et al. [35] prepared green titanium dioxide NPs using leaf extract of the biodiesel plant, *Jatropha curcas* L., and evaluated its performance for the photocatalytic treatment of TWW after the secondary (biological) treatment process, achieving 82.26% and 76.48% of COD and Cr removal, respectively, in a parabolic trough reactor (PTR). Also, Jegadeeswaran et al. [36] proposed a novel green synthesis of Ag/TiO_2 nanocomposites of anatase phase and average particles size of 25.74 nm from *Padina tetrastromatica* extract.

Accordingly, the present work is focused on the study of the synthesis and structural characterization of the Fe-doped TiO_2 nanoparticles prepared by green synthesis. The main aim is to determine the effect of the introduction of the doping elements in the optical, physicochemical, structural, and morphological properties. Nanostructured TiO_2 anatase doped with different Fe : Ti molar ratios were successfully synthesized. The prepared samples were characterized by photoluminescence, cathodoluminescence, UV-Vis spectrophotometry of diffuse reflectance, Raman spectroscopy, XRD, SEM-EDS, and TEM-SAED.

2. Materials and Methods

2.1. Materials. Fresh lemongrass plant leaves (*Cymbopogon citratus*) were collected from Cartagena, Colombia. Titanium(IV) isopropoxide ($C_{12}H_{28}O_4Ti$) solution (95%) and iron(III) chloride hexahydrate (98% purity) were purchased from Alfa Aesar® and Panreac, respectively. All reactions were carried out using ACS Reagent chemicals.

2.2. Lemongrass Leaf Extract Preparation. The lemongrass leaves were washed with griffin water. Then, they were dried for six hours in an air circulation oven at 60°C (Esco Isotherm®, OFA 32-8) and crushed using a manual mill. The dried and crushed biomass (100 g) was placed in cloth bags and subjected to a solvent extraction process using a Soxhlet extractor for 6 h in approximately 500 mL of distilled water [37, 38]. The extract was stored in the refrigerator at 4°C. Further, this extract was used to synthesize TiO_2 nanoparticles [33]. The extraction-concentration was performed using the technique solid-phase microextraction (SPME), monitoring in vapor phase (HS), using a fiber of fused silica coated with PDMS/DVB of thickness 65 micrometers (PDMS/DVB-65 pm). The chromatographic analysis was carried out in an AT 6890 Series Plus gas chromatograph (Agilent Technologies, Palo Alto, California, USA), coupled to a selective mass detector (Agilent Technologies, MSD 5973), operated in the scanning complete radio frequency mode (*full scan*). The column used in the analysis was DB-5MS (5% phenyl-poly (methylsiloxane), 60 m × 0.25 mm × 0.25 m). The injection was done in the split mode (30 : 1) with the SPME device.

2.3. Green Synthesis of Fe-TiO_2 Nanoparticles. In a typical experiment, the reaction was carried out in a 250 mL beaker, which was introduced in an ultrasound processor (ultrasonic processor, WiseClean WUC-A06H, 60 Hz). Twenty milliliters of the precursor agent (titanium isopropoxide) was added to 100 mL of the aqueous extract of lemongrass contained in a burette, at a rate of 1 mL·s^{-1}; additionally, the reaction lasted approximately 30 minutes with constant agitation, making use of a stirring rod [18, 33]. The nanoparticles were washed with 70% vol. ethanol and finally with distilled water, using separation by centrifugation (universal centrifuge PLC-012E) for 15 min at 5000 rpm. The synthesized titanium dioxide nanoparticles were calcined at 550°C for 3 hours in a Thermo Scientific FB1415M-1450 W-50/60 Hz muffle [39].

2.4. Characterization. CL measurements were performed in Hitachi S2500 SEM at room temperatures using a Hamamatsu photonic multichannel analyzer PMA-12 with excitation voltage of 25 kV. HORIBA Jobin Yvon LabRAM HR800 UV-Vis used the Olympus BX41 confocal microscope was used in photoluminescence (PL) and Raman measurements. PL spectra have been acquired with a 325 nm He-Cd laser using the lowest laser intensity (0.1 I_0) to avoid the anatase to rutile phase transformation during the PL acquisition; morever a filter D1, hole 850 μm, spectrometer 327,199 nm, and ×40 objective were used for the photoluminescence study; while μ-Raman spectroscopy has been performed using a red He-Ne laser of 633 nm wavelength. The UV-Vis absorption studies of the photocatalysts were conducted on UV-Vis diffuse reflectance spectrophotometer (Thermo Scientific EVOLUTION-600), with $BaSO_4$ as reference. The samples were studied by X-ray diffraction (XRD) using a Panalytical X'Pert Pro Alpha1 instrument, which is equipped with a primary fast X'Celerator detector operating at 45 kV and 40 mA and fitted with a primary curved Ge 111 monochromator to obtain CuKα1 radiation ($\lambda = 1.5406$ Å). Data were collected at 2θ between 10° and 90°, with a step size of 0.04°·s^{-1}. SEM micrographs and energy-dispersive X-ray spectroscopy (EDS) maps were obtained in a Leica 440 SEM coupled to Bruker AXS XFlash Detector 4010. Investigation of particle morphology of Fe^{3+}-doped TiO_2 samples was performed on a JEM 2100HT JEOL transmission electron microscope (TEM) provided with 200 kV emission gun, beam current of 108.6 μA, and equipped with diffraction mode (camera length of 300 mm) for selected area electron diffraction (SAED). The samples were prepared by ultrasonic dispersing of the powders as slurry in 2-propanol and deposited in TEM grids.

3. Results and Discussion

3.1. Lemongrass Leaf Composition. The lemongrass plant is formed by a variety of chemical components with higher predominance terpenes and terpenoids associated with aldehydes, alcohols, and ketones [40]. To guarantee the formation of the titanium dioxide nanoparticles, it is necessary that the extract of the lemongrass plant has phytochemical components that guarantee the reduction of the titanium (IV) isopropoxide precursor [41]. Figure 1 shows the chromatogram obtained for the lemongrass sample. The presumptive identification of the compounds registered in solid sample was their mass spectra (EI, 70 eV), using the Adams and Wiley databases. In Table 1, appear the presumptive identification and relative quantity (%) of the components present in lemongrass solid sample analyzed by GC-MS operated in the full-scan mode of radio frequency. In order to guarantee the formation of TiO_2 nanoparticles with sizes of less than 20 nm, it is necessary that the extract of the lemongrass leaves has phytochemical components that act as surfactants and stabilizers that prevent excessive agglomeration of the nanoparticulate material formed during the synthesis [33, 35, 41–47], as proposed in the mechanism shown in Figure 2. However, it is possible to synthesize TiO_2 powders through the complete hydrolysis of the used precursor (titanium isopropoxide) through the direct contact of the titanium source with water [45, 48], with the disadvantage that it does not present alternatives to control the stages of nucleation and growth that are carried out in the process of production of nanoparticles in solution [49].

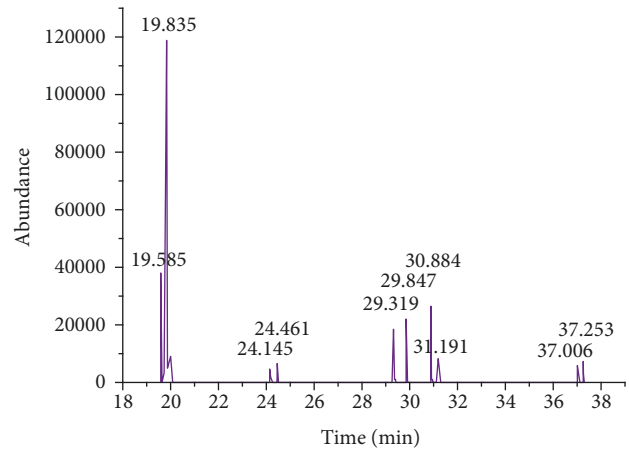

Figure 1: GC-MS chromatogram for lemongrass leaves.

Table 1: Presumptive identification and relative quantity (%) of the components present in lemongrass biomass.

t_R (min)	Tentative identification	Relative quantity (%)
19.59	6-Methyl-5-hepten-2-one	14.9
19.84	β-Myrcene	44.5
24.15	NI, compound M^+ 150	1.6
24.46	NI, compound M^+ 150	2.7
29.32	NI, compound M^+ 154	7.2
29.85	Neral	9.0
30.88	Geranial	12.2
31.19	NI, compound M^+ 150	2.9
37.01	NI	2.0
37.25	NI[a]	2.9

[a]Unidentified compound.

3.2. XRD. The XRD pattern synthesized TiO_2 nanoparticles using the leaf extract of the lemongrass plant (*Cymbopogon citratus*) is depicted in Figure 3. The ten distinct peaks at 2θ = 25.61°, 37.8°, 38.10°, 48.47°, 54.24°, 55.36°, 62.99°, 69.20°, 70.59°, and 75.47° in the XRD pattern of Fe^{3+}-doped TiO_2 and undoped nanopowders are consistent with anatase (101), (103), (004), (200), (105), (211), (204), (116), (220), and (107) lattice planes (JCPDS No. 21-1272). The diffraction peaks corresponding to rutile phase only appeared in Degussa (Evonik) P-25 at 2θ = 27.58°, 36.30°, and 54.42° can be attributed to (110), (101), and (211) planes of rutile TiO_2 (JCPDS Card No. 21-1276). The sharpness of peaks and the absence of unidentified peaks confirmed the crystalline and high purity of nanoparticles prepared. The average crystalline size of TiO_2 nanoparticles was calculated using Debye–Scherrer's equation [33]:

$$D = \frac{K\lambda}{\beta \cos \theta}, \quad (1)$$

where D is the average crystal size in Å, λ is the wavelength of the X-ray radiation (1.5406 Å), K is the dimensionless shape factor (0.9), β is the line width at half-maximum intensity (FWHM) in radians, and θ is Bragg's angle in degrees [35].

The average crystalline size was estimated from the FWHM of the TiO_2 main peak (2θ = 25.61°) of XRD patterns, which corresponds to the plane (101). The average crystalline size was around 10 nm for the prepared nanomaterials. Iron (Fe^{+3}) can conveniently integrate into the matrix of TiO_2 owing its atomic radius of 0.69 Å which is almost equal to Ti^{+4} atomic radius of 0.745 Å [50]. However, no reduction in crystalline size is observed, which is attributed to nanoparticles growth in the calcination process of the wet impregnation at 350°C for 3 h. Table 2 summarizes the results obtained for the diameter by Debye–Scherrer's equation.

3.3. Raman Spectroscopy. Micro-Raman spectroscopy has been carried out for further analysis of the structural phases of pure and Fe-doped TiO_2 NPs, as shown in Figure 4. Anatase phase of titanium dioxide has six Raman active modes $A_{1g} + 2B_{1g} + 3E_g$ at 144 cm^{-1} (E_g), 197 cm^{-1} (E_g), 399 cm^{-1} (B_{1g}), 516 cm^{-1} ($A_{1g} + B_{1g}$), and 639 cm^{-1} (E_g), which were identified on the Raman spectra of all the samples under discussion [51]. It has been shown that any peak associated with iron oxide are not observed, even with a highly doped sample. This means that Raman spectral observations are in good agreement with the XRD results. Moreover, Fe-doped TiO_2 NPs retained the anatase structure, which indicates that the Fe^{+3} dopants are successfully incorporated into the TiO_2 framework, replacing Ti^{+4} cations. However, it has been observed that the Raman band at 144 cm^{-1} (inset in Figure 4) tends to shift to a higher Raman intensity as the amount of the Fe dopant increases.

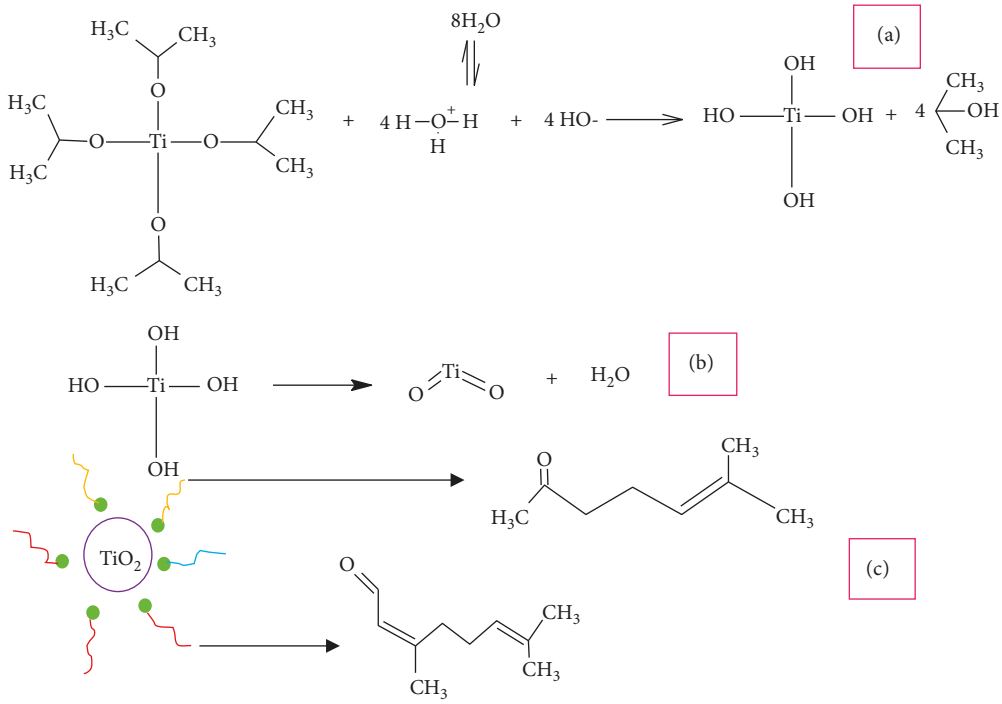

Figure 2: (a) Complete hydrolysis of the precursor; (b) condensation; (c) encapsulation/stabilization by the phytochemicals present in the aqueous extract of lemongrass (6-methyl-5-hepten-2-ona, neral, and geranial).

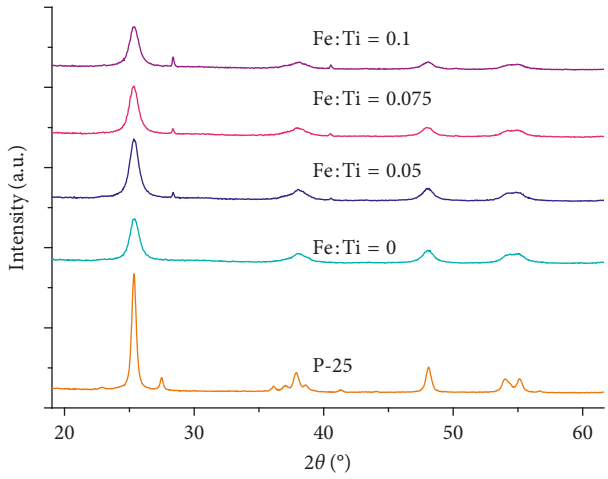

Figure 3: XRD spectra of TiO_2 and Fe-TiO_2 with different Fe^{3+} : Ti molar ratio calcined at 550°C for 3 h.

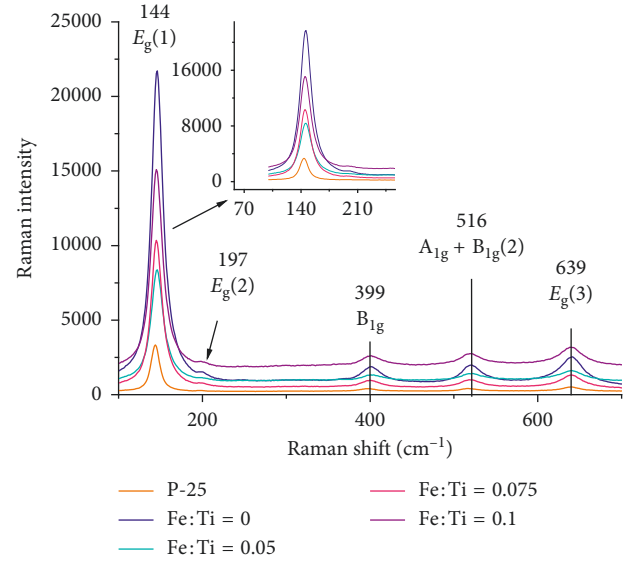

Figure 4: Raman spectra of TiO_2 and Fe-TiO_2 with different Fe^{3+} : Ti molar ratios.

Table 2: Particle size obtained for the diameter by Debye–Scherrer's equation.

Sample	Particle size (Debye–Scherrer's equation) (nm)
P-25	19.72
Fe : Ti = 0	9.37
Fe : Ti = 0.05	10.33
Fe : Ti = 0.075	10.13
Fe : Ti = 0.1	9.91

Generally, it has been accepted that shifts in the Raman peak occur because of changes in the structure, particle size, the nature of defects, and so on [52].

3.4. Cathodoluminescence (CL) and Photoluminescence (PL). The spectra of the cathodoluminescence detector and photoluminescence obtained for all prepared materials are shown in Figures 5 and 6, respectively. For both cases in the emission (visible spectrum, 380–700 nm) of all samples studied clearly identified the presence of a broadband around the 500–550 nm, which is due to the existence of surface states and the self-trapped excites in the anatase phase.

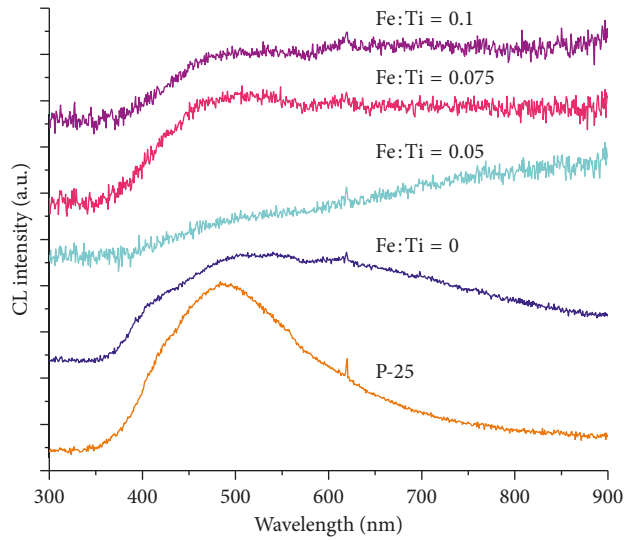

Figure 5: CL measurements of TiO_2 and Fe-TiO_2 with different Fe^{3+} : Ti molar ratios.

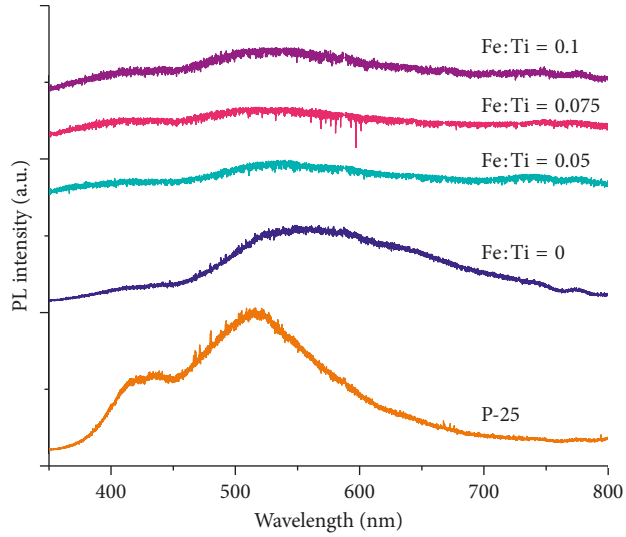

Figure 6: PL measurements of TiO_2 and Fe-TiO_2 with different Fe^{3+} : Ti molar ratios.

Also, it is evident the existence of a shoulder 600–650 nm related to the oxygen vacancies in the involved phase, similar to what was reported by several authors [53, 54]. On the other hand, it is noticeable that there is difference in the intensity of the luminescence, which indicates inhibition of the recombination of the electron/hole pairs photogenerated by the ions of Fe^{3+}. The intensity of Fe-TiO_2 is lower than that of pure TiO_2, which suggests that electron-hollow recombination is much lower, and the effectiveness of separation is much higher. The decrease in the rate of recombination implies that a large number of electrons and photogenerated gaps are involved in the photochemical transformation, which coincides with the reported by other researchers [9, 22, 39, 52, 55].

3.5. TEM-SAED. The surface morphology and particle size (size distribution) of the pure (Fe : Ti = 0) and Fe-doped TiO_2 (Fe : Ti = 0.1) photocatalyst were further analyzed by TEM, as shown in Figures 7(a) and 7(b), respectively.

It is evident from these images that the synthesized nanoparticles were agglomerated, and their shapes were quasi-nanospheres; this corresponds to the results reported by several authors in research related to the green synthesis of TiO_2 by the use of aqueous extracts of leaves [33–35]. Also, it can be seen that particles have a small size but are perfectly crystalline in nature. The TEM results are in close agreement with the average crystallite size obtained from the XRD pattern. The average particle size increases for Fe : Ti = 0.1 as compared to pure TiO_2, which is attributed to nanoparticles growth in the calcination process of the wet impregnation at 350°C for 3 h. The structural information obtained from SAED (Figure 8) pattern shows the polycrystalline nature of Fe-TiO_2 nanoparticles (Fe : Ti = 0.1), which is indicated by the (101), (004), (200), and (105) planes of the anatase phase, similar to that reported by Ali et al. [52]. The interplanar space was determined through Equation (2), where, h, k, and l are the Miller indexes, a and c are the network parameters for a tetragonal structure (anatase), and $a = 3{,}7852 = b \neq c = 9{,}5139$ and $d_{(hkl)}$ is the interplanar distance value in Å [9, 17].

$$\frac{1}{d^2_{(hkl)}} = \frac{h^2 + k^2}{a^2} + \frac{l^2}{c^2}. \quad (2)$$

3.6. SEM-EDS. The SEM micrographs and EDS analysis of the pure (P-25 and Fe : Ti = 0) and Fe-doped TiO_2 (Fe : Ti = 0.05, Fe : Ti = 0.075, and Fe : Ti = 0.1) photocatalyst are depicted in Figures 9(a)–9(e), respectively. Pure and Fe^{3+}-doped TiO_2 are ultrafine, so they are coupled and agglomerate due to the high surface energy [50]. This means that the green synthesis method can lead to the creation of the product with agglomerates in the micrometric scale, for which irregular forms are observed, similar to what was reported by Arabi et al. [31] for the green synthesis of TiO_2 using the extract of Moose and Thyme.

The compositional analysis shows the separate peak of titanium (Ti, 4.508 keV), iron (Fe, 6.398 keV), oxygen (O, 0.523 keV), and other elements as Na, Ca, Si, Cl, and K, which come from the water used in the synthesis process [56]. Table 3 shows the atomic percentages obtained for each element by EDS, in addition to the impregnation efficiencies achieved for all prepared samples.

3.7. UV-Vis DRS. The UV-Vis diffuse reflectance spectra of the pure TiO_2 and Fe-TiO_2 samples are shown in Figure 10. The absorption is enhanced in the visible light region when Fe is doped into TiO_2. The Fe-TiO_2 samples exhibit absorption in both the UV and visible light regions. Obviously, the diffuse reflectance spectra of all the Fe-TiO_2 nanostructures exhibit increased absorption in the visible light

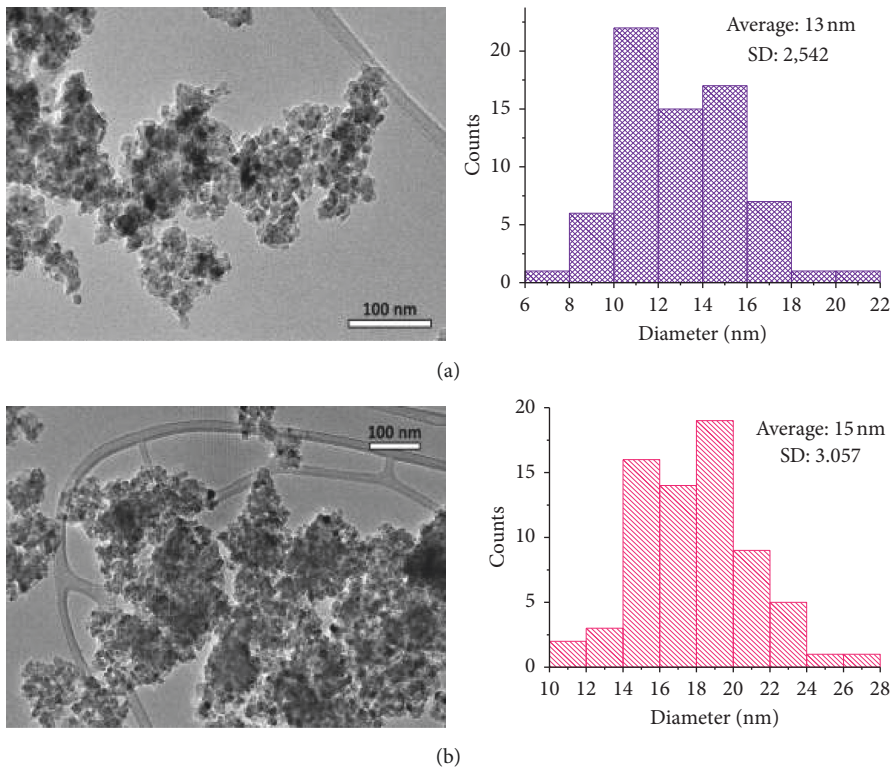

Figure 7: TEM images and particle size distribution of (a) Fe : Ti = 0 and (b) Fe : Ti = 0.

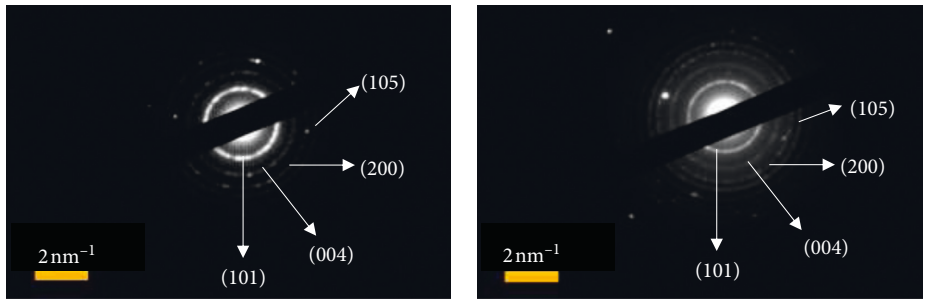

Figure 8: SAED pattern of (a) pure TiO_2 and (b) Fe-TiO_2 nanoparticles (Fe : Ti = 0.1).

range; also, this increase is more evident by increasing the relationship molar Fe : Ti, which is induced by the electron transition from Fe 3d orbitals to TiO_2 conduction band (CB) from the O 2p TiO_2 valence band (VB), generating a considerable decrease in the band gap energy of TiO_2 [18]. In summary, doping Fe^{3+} causes structural defects of crystal lattice to introduce impurity or defect energy level and induces the local states below the conduction band edge and then results in this redshift and narrows the band gap [20]. Although doping of the Fe ions in the TiO_2 does not modify the position of the valence band edge of the TiO_2, it introduces new energy levels (Fe^{3+}/Fe^{4+}) of the transition Fe ions into the band gap of the TiO_2.

The direct band gap energy (E_g) was calculated using the following Tauc plot as given in the following equation, which is derived assuming a direct transition between the edge of the valence band and conduction:

$$(\alpha h\nu)^{1/n} = A\left(h\nu - E_g\right), \tag{3}$$

where $h\nu$ is the photon energy, a is the absorption coefficient, and A is an energy-dependent constant and known as the band tailing parameter. Another constant is n, which is known as power factor of the transition mode of the materials.

The values of n for direct, indirect, direct forbidden, and indirect forbidden transitions are 1/2, 2, 3/2, and 3, respectively. The pure anatase and Degussa P-25 TiO_2 used in this research are considered as direct band gap materials [57, 58]. Therefore, the value of n was taken 1/2 to plot the graph $(\alpha h\nu)^2$ versus $h\nu$ as shown in Figure 11. It is observed a

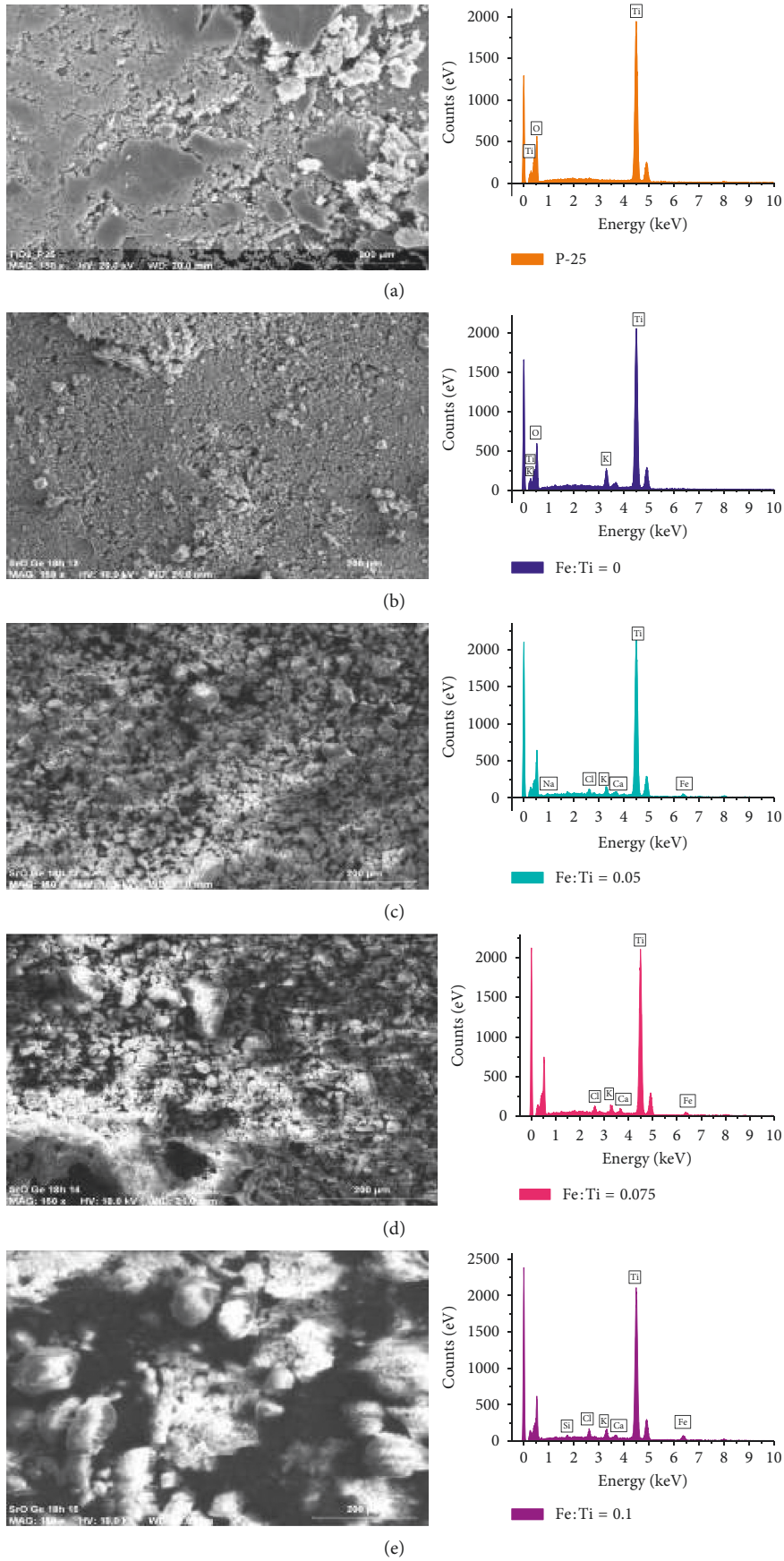

FIGURE 9: SEM micrographs and EDS spectrum of (a) P-25 TiO_2, (b) Fe : Ti = 0, (c) Fe : Ti = 0.05, (d) Fe : Ti = 0.075, and (e) Fe : Ti = 0.1; magnification: 150x.

Table 3: Atomic percentages and doping impregnation efficiency obtained EDS analysis.

Sample	Ti (atm.%)	O (atm.%)	Fe (atm.%)	Impregnation efficiency (%)
P-25	37.73 ± 1.7	62.27 ± 39.9	—	—
Fe : Ti = 0	37.77 ± 1.8	59.15 ± 35.2	—	—
Fe : Ti = 0.05	39.08 ± 1.8	59.63 ± 35.7	1.30 ± 0.1	66.53
Fe : Ti = 0.075	37.32 ± 1.9	61.12 ± 35.6	1.56 ± 0.2	55.73
Fe : Ti = 0.1	40.59 ± 2.0	57.05 ± 35.1	2.37 ± 0.2	58.38

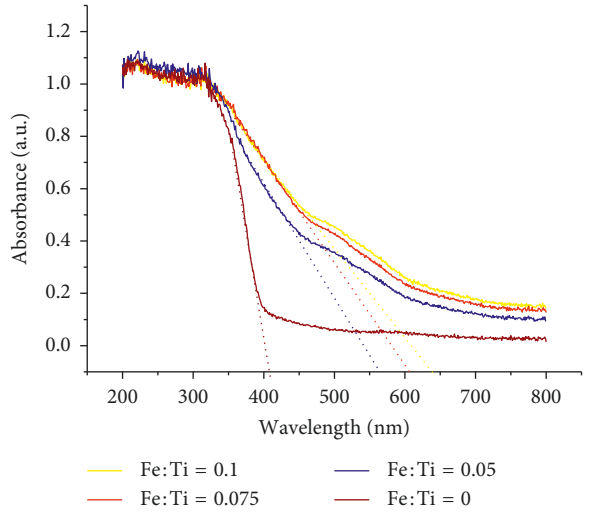

Figure 10: Typical UV-Vis spectra of bare TiO_2 and Fe-TiO_2.

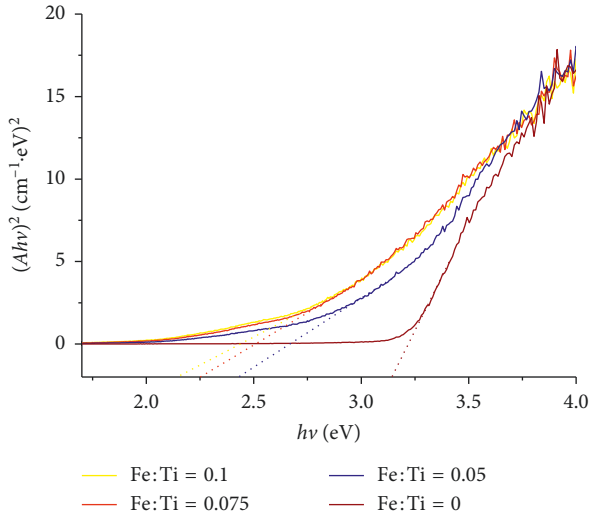

Figure 11: Tauc plot analysis of bare TiO_2 and Fe-TiO_2.

reduction of 1 eV for the material Fe : Ti = 0.1 in comparison with the pure TiO_2 (Fe : Ti = 0) synthesized by the methodology of green chemistry assisted by ultrasound, which would allow to use more efficiently the solar radiation in heterogeneous photocatalytic processes for the degradation of organic pollutants. These results relate to several recent research focused on the doping of titanium dioxide with Fe^{3+} ions [56, 59–61]. Moradi et al. [18] observed the decrease of the band gap with the increase of the relationship molar Fe : Ti in catalysts of TiO_2 doped with Fe^{3+} using the technique sol-gel.

4. Conclusions

In summary, TiO_2 (anatase phase only) doped with a different molar ratio Fe^{3+} : Ti was successfully prepared via green synthesis (using the leaves extract of lemongrass plant leaves) assisted ultrasound method followed by calcination. The average crystalline size calculated by XRD pattern was between 9.37 to 10.33 for the TiO_2 (Fe : Ti = 0) and TiO_2 (Fe : Ti = 0.05) samples, respectively. The scanning electron microscopy with energy-dispersive X-ray (SEM-EDS) shows nanoparticles clusters and efficiencies of impregnations between 66.5 and 58.4% depending on the theoretical dopant amount. From PL and CL studies, it was confirmed that doping of Fe (III) ions into TiO_2 matrix leads to the inhibition of recombination of charge carriers, thereby enhancing photochemical quantum efficiency. From UV-Vis DRS analysis, a reduction of 1 eV was observed for the material Fe : Ti = 0.1 in comparison with the pure TiO_2 (Fe : Ti = 0) synthesized by the methodology of green chemistry assisted by ultrasound, which would allow to use more efficiently the solar radiation in heterogeneous photocatalytic processes for the degradation of organic pollutants.

Data Availability

The data used to support the findings of this study are available from the corresponding author upon request.

Conflicts of Interest

The authors declare that there are no conflicts of interest regarding the publication of this paper.

Acknowledgments

The authors greatly acknowledge the financial support from University de Cartagena (International Internship 2017, 01735) and the Colombian Administrative Department of Science, Technology and Innovation (Colciencias Young Researchers Program 2017). The authors would also like to thank the Electronic Nanomaterials Physics Research group of Universidad Complutense de Madrid for providing the facility of all the equipment used in this research.

References

[1] Q. Deng, Y. Liu, K. Mu et al., "Preparation and characterization of F-modified C-TiO_2 and its photocatalytic

properties," *Physica Status Solidi (A)*, vol. 212, no. 3, pp. 691–697, 2015.

[2] K. S. Prasad, A. Patra, G. Shruthi, and S. Chandan, "Aqueous extract of *Saraca indica* leaves in the synthesis of copper oxide nanoparticles: finding a way towards going green," *Journal of Nanotechnology*, vol. 2017, Article ID 7502610, 6 pages, 2017.

[3] X. Wang, X. Cheng, X. Yu, and X. Quan, "Study on surface-enhanced Raman scattering substrate based on titanium oxide nanorods coated with gold nanoparticles," *Journal of Nanotechnology*, vol. 2018, Article ID 9602480, 9 pages, 2018.

[4] W. Sangchay, "WO_3-doped TiO_2 coating on charcoal activated with increase photocatalytic and antibacterial properties synthesized by microwave-assisted sol-gel method," *Journal of Nanotechnology*, vol. 2017, Article ID 7902930, 7 pages, 2017.

[5] W. Chakhari, J. Ben Naceur, S. Ben Taieb, I. Ben Assaker, and R. Chtourou, "Fe-doped TiO_2 nanorods with enhanced electrochemical properties as efficient photoanode materials," *Journal of Alloys and Compounds*, vol. 708, pp. 862–870, 2017.

[6] T. Kaur, A. Sraw, R. K. Wanchoo, and A. P. Toor, "Visible–light induced photocatalytic degradation of fungicide with Fe and Si doped TiO_2 nanoparticles," *Materials Today: Proceedings*, vol. 3, no. 2, pp. 354–361, 2016.

[7] Maulidiyah, T. Azis, A. T. Nurwahidah, D. Wibowo, and M. Nurdin, "Photoelectrocatalyst of Fe co-doped N-TiO_2/Ti nanotubes: pesticide degradation of thiamethoxam under UV–visible lights," *Environmental Nanotechnology, Monitoring & Management*, vol. 8, pp. 103–111, 2017.

[8] Q. Wang, R. Jin, M. Zhang, and S. Gao, "Solvothermal preparation of Fe-doped TiO_2 nanotube arrays for enhancement in visible light induced photoelectrochemical performance," *Journal of Alloys and Compounds*, vol. 690, pp. 139–144, 2017.

[9] C. W. Soo, J. C. Juan, C. W. Lai, S. B. A. Hamid, and R. M. Yusop, "Fe-doped mesoporous anatase-brookite titania in the solar-light-induced photodegradation of Reactive Black 5 dye," *Journal of the Taiwan Institute of Chemical Engineers*, vol. 68, pp. 153–161, 2016.

[10] W. Mekprasart, S. Suphankij, T. Tangcharoen, A. Simpraditpan, and W. Pecharapa, "Modification of dye-sensitized solar cell working electrode using TiO_2 nanoparticle/N-doped TiO_2 nanofiber composites," *Physica Status Solidi (A)*, vol. 211, no. 8, pp. 1745–1751, 2014.

[11] Z. Wu, Z.-K. Zhang, D.-Z. Guo, Y.-J. Xing, and G.-M. Zhang, "Titanium oxide nanospheres: preparation, characterization, and wide-spectral absorption," *Physica Status Solidi (A)*, vol. 209, no. 10, pp. 2020–2026, 2012.

[12] K. Kalantari, M. Kalbasi, M. Sohrabi, and S. J. Royaee, "Enhancing the photocatalytic oxidation of dibenzothiophene using visible light responsive Fe and N co-doped TiO_2 nanoparticles," *Ceramics International*, vol. 43, no. 1, pp. 973–981, 2017.

[13] S. Larumbe, M. Monge, and C. Gómez-Polo, "Comparative study of (N, Fe) doped TiO_2 photocatalysts," *Applied Surface Science*, vol. 327, pp. 490–497, 2015.

[14] P. Huo, Z. Lu, H. Wang et al., "Enhanced photodegradation of antibiotics solution under visible light with Fe^{2+}/Fe^{3+} immobilized on TiO_2/fly-ash cenospheres by using ions imprinting technology," *Chemical Engineering Journal*, vol. 172, no. 2-3, pp. 615–622, 2011.

[15] E. Márquez Brazón, C. Piccirillo, I. S. Moreira, and P. M. L. Castro, "Photodegradation of pharmaceutical persistent pollutants using hydroxyapatite-based materials," *Journal of Environmental Management*, vol. 182, pp. 486–495, 2016.

[16] L. Schlur, S. Begin-Colin, P. Gilliot et al., "Effect of ball-milling and Fe-/Al-doping on the structural aspect and visible light photocatalytic activity of TiO_2 towards *Escherichia coli* bacteria abatement," *Materials Science and Engineering: C*, vol. 38, no. 1, pp. 11–19, 2014.

[17] M. Yeganeh, N. Shahtahmasebi, A. Kompany et al., "The magnetic characterization of Fe doped TiO_2 semiconducting oxide nanoparticles synthesized by sol–gel method," *Physica B: Condensed Matter*, vol. 511, pp. 89–98, 2017.

[18] H. Moradi, A. Eshaghi, S. R. Hosseini, and K. Ghani, "Fabrication of Fe-doped TiO_2 nanoparticles and investigation of photocatalytic decolorization of reactive red 198 under visible light irradiation," *Ultrasonics Sonochemistry*, vol. 32, pp. 314–319, 2016.

[19] M. Pazoki, M. Parsa, and R. Farhadpour, "Removal of the hormones dexamethasone (DXM) by Ag doped on TiO_2 photocatalysis," *Journal of Environmental Chemical Engineering*, vol. 4, no. 4, pp. 4426–4434, 2016.

[20] Q. Wang, C. Yang, G. Zhang, L. Hu, and P. Wang, "Photocatalytic Fe-doped TiO_2/PSF composite UF membranes: characterization and performance on BPA removal under visible-light irradiation," *Chemical Engineering Journal*, vol. 319, pp. 39–47, 2017.

[21] N. C. Birben, C. S. Uyguner-Demirel, S. S. Kavurmaci et al., "Application of Fe-doped TiO_2 specimens for the solar photocatalytic degradation of humic acid," *Catalysis Today*, vol. 281, pp. 78–84, 2017.

[22] S. A. Ahmed, "Ferromagnetism in Cr-, Fe-, and Ni-doped TiO_2 samples," *Journal of Magnetism and Magnetic Materials*, vol. 442, pp. 152–157, 2017.

[23] Y. Sui, Q. Liu, T. Jiang, and Y. Guo, "Synthesis of nano-TiO_2 photocatalysts with tunable Fe doping concentration from Ti-bearing tailings," *Applied Surface Science*, vol. 428, pp. 1149–1158, 2018.

[24] V. Moradi, M. B. G. Jun, A. Blackburn, and R. A. Herring, "Significant improvement in visible light photocatalytic activity of Fe doped TiO_2 using an acid treatment process," *Applied Surface Science*, vol. 427, pp. 791–799, 2018.

[25] E. Craciun, L. Predoana, I. Atkinson et al., "Fe^{3+}-doped TiO_2 nanopowders for photocatalytic mineralization of oxalic acid under solar light irradiation," *Journal of Photochemistry and Photobiology A: Chemistry*, vol. 356, pp. 18–28, 2018.

[26] M. Zare, K. Namratha, M. S. Thakur, and K. Byrappa, "Biocompatibility assessment and photocatalytic activity of bio-hydrothermal synthesis of ZnO nanoparticles by *Thymus vulgaris* leaf extract," *Materials Research Bulletin*, vol. 109, pp. 49–59, 2019.

[27] S. Shalini, R. Balasundaraprabhu, T. Satish Kumar et al., "Enhanced performance of sodium doped TiO_2 nanorods based dye sensitized solar cells sensitized with extract from petals of *Hibiscus sabdariffa* (Roselle)," *Materials Letters*, vol. 221, pp. 192–195, 2018.

[28] A. A. Kashale, K. P. Gattu, K. Ghule et al., "Biomediated green synthesis of TiO_2 nanoparticles for lithium ion battery application," *Composites Part B: Engineering*, vol. 99, pp. 297–304, 2016.

[29] S. Shalini, N. Prabavathy, R. Balasundaraprabhu et al., "Studies on DSSC encompassing flower shaped assembly of Na-doped TiO_2 nanorods sensitized with extract from petals of *Kigelia africana*," *Optik*, vol. 155, pp. 334–343, 2018.

[30] S. Subhapriya and P. Gomathipriya, "Green synthesis of titanium dioxide (TiO_2) nanoparticles by *Trigonella foenum-graecum* extract and its antimicrobial properties," *Microbial Pathogenesis*, vol. 116, pp. 215–220, 2018.

[31] N. Arabi, A. Kianvash, A. Hajalilou, and E. Abouzari-lotf, "A facile and green synthetic approach toward fabrication of Alcea- and Thyme-stabilized TiO_2 nanoparticles for photocatalytic applications," *Arabian Journal of Chemistry*, 2018, In press.

[32] M. Atarod, M. Nasrollahzadeh, and S. Mohammad Sajadi, "Euphorbia heterophylla leaf extract mediated green synthesis of Ag/TiO_2 nanocomposite and investigation of its excellent catalytic activity for reduction of variety of dyes in water," *Journal of Colloid and Interface Science*, vol. 462, pp. 272–279, 2016.

[33] M. Sundrarajan, K. Bama, M. Bhavani et al., "Obtaining titanium dioxide nanoparticles with spherical shape and antimicrobial properties using *M. citrifolia* leaves extract by hydrothermal method," *Journal of Photochemistry and Photobiology B: Biology*, vol. 171, pp. 117–124, 2017.

[34] P. Rajiv, C. Jayaseelan, C. Kamaraj, S. R. R. Rajasree, and R. Regina, "In vitro antimalarial activity of synthesized TiO_2 nanoparticles using *Momordica charantia* leaf extract against *Plasmodium falciparum*," *Journal of Applied Biomedicine*, vol. 16, no. 4, pp. 378–386, 2018.

[35] S. P. Goutam, G. Saxena, V. Singh, A. K. Yadav, R. N. Bharagava, and K. B. Thapa, "Green synthesis of TiO_2 nanoparticles using leaf extract of *Jatropha curcas* L. for photocatalytic degradation of tannery wastewater," *Chemical Engineering Journal*, vol. 336, pp. 386–396, 2018.

[36] P. Jegadeeswaran, P. Rajiv, P. Vanathi, S. Rajeshwari, and R. Venckatesh, "A novel green technology: synthesis and characterization of Ag/TiO_2 nanocomposites using *Padina tetrastromatica* (seaweed) extract," *Materials Letters*, vol. 166, pp. 137–139, 2016.

[37] B. Balakrishnan, S. Paramasivam, and A. Arulkumar, "Evaluation of the lemongrass plant (*Cymbopogon citratus*) extracted in different solvents for antioxidant and antibacterial activity against human pathogens," *Asian Pacific Journal of Tropical Disease*, vol. 4, pp. S134–S139, 2014.

[38] T. S. Geetha and N. Geetha, "Phytochemical screening, quantitative analysis of primary and secondary metabolites of *Cymbopogan citratus* (DC) stapf. Leaves from Kodaikanal hills, Tamilnadu," *International Journal of PharmTech Research*, vol. 6, no. 2, pp. 521–529, 2014.

[39] S. Sood, A. Umar, S. K. Mehta, and S. K. Kansal, "Highly effective Fe-doped TiO_2 nanoparticles photocatalysts for visible-light driven photocatalytic degradation of toxic organic compounds," *Journal of Colloid and Interface Science*, vol. 450, pp. 213–223, 2015.

[40] L. Venzon, L N. B. Mariano, L. B. Somensi et al., "Essential oil of *Cymbopogon citratus* (lemongrass) and geraniol, but not citral, promote gastric healing activity in mice," *Biomedicine & Pharmacotherapy*, vol. 98, pp. 118–124, 2018.

[41] M. Nasrollahzadeh and S. M. Sajadi, "Synthesis and characterization of titanium dioxide nanoparticles using Euphorbia heteradena Jaub root extract and evaluation of their stability," *Ceramics International*, vol. 41, no. 10, pp. 14435–14439, 2015.

[42] G. Rajakumar, A. A. Rahuman, B. Priyamvada, V. G. Khanna, D. K. Kumar, and P. J. Sujin, "*Eclipta prostrata* leaf aqueous extract mediated synthesis of titanium dioxide nanoparticles," *Materials Letters*, vol. 68, pp. 115–117, 2012.

[43] T. Santhoshkumar, A. A. Rahuman, C. Jayaseelan et al., "Green synthesis of titanium dioxide nanoparticles using *Psidium guajava* extract and its antibacterial and antioxidant properties," *Asian Pacific Journal of Tropical Medicine*, vol. 7, no. 12, pp. 968–976, 2014.

[44] V. Sivaranjani and P. Philominathan, "Synthesize of Titanium dioxide nanoparticles using *Moringa oleifera* leaves and evaluation of wound healing activity," *Wound Medicine*, vol. 12, pp. 1–5, 2016.

[45] P. Verma and S. K. Samanta, "Continuous ultrasonic stimulation based direct green synthesis of pure anatase-TiO_2 nanoparticles with better separability and reusability for photocatalytic water decontamination," *Materials Research Express*, vol. 5, no. 6, pp. 49–65, 2018.

[46] K. Logaranjan, A. J. Raiza, S. C. B. Gopinath, Y. Chen, and K. Pandian, "Shape- and size-controlled synthesis of silver nanoparticles using *Aloe vera* plant extract and their antimicrobial activity," *Nanoscale Research Letters*, vol. 11, no. 1, p. 520, 2016.

[47] N. K. R. Bogireddy, U. Pal, L. M. Gomez, and V. Agarwal, "Size controlled green synthesis of gold nanoparticles using *Coffea arabica* seed extract and their catalytic performance in 4-nitrophenol reduction," *RSC Advances*, vol. 8, no. 44, pp. 24819–24826, 2018.

[48] M. Kinoshita and Y. Shimoyama, "Photocatalytic activity of mixed-phase titanium oxide synthesized by supercritical sol-gel reaction," *Journal of Supercritical Fluids*, vol. 138, pp. 29–35, 2018.

[49] C. M. Phan and H. M. Nguyen, "Role of capping agent in wet synthesis of nanoparticles," *Journal of Physical Chemistry A*, vol. 121, no. 17, pp. 3213–3219, 2017.

[50] R. Ambati and P. R. Gogate, "Ultrasound assisted synthesis of iron doped TiO_2 catalyst," *Ultrasonics sonochemistry*, vol. 40, pp. 91–100, 2018.

[51] A. G. Ilie, M. Scarisoareanu, I. Morjan, E. Dutu, M. Badiceanu, and I. Mihailescu, "Principal component analysis of Raman spectra for TiO_2 nanoparticle characterization," *Applied Surface Science*, vol. 417, pp. 93–103, 2017.

[52] T. Ali, P. Tripathi, A. Azam et al., "Photocatalytic performance of Fe-doped TiO_2 nanoparticles under visible-light irradiation," *Materials Research Express*, vol. 4, no. 1, article 015022, 2017.

[53] M. Barberio, P. Barone, V. Pingitore, and A. Bonanno, "Optical properties of TiO_2 anatase—carbon nanotubes composites studied by cathodoluminescence spectroscopy," *Superlattices and Microstructures*, vol. 51, no. 1, pp. 177–183, 2012.

[54] M. Enachi, M. A. Stevens-Kalceff, A. Sarua, V. Ursaki, and I. Tiginyanu, "Design of titania nanotube structures by focused laser beam direct writing," *Journal of Applied Physics*, vol. 114, no. 23, article 234302, 2013.

[55] L. Lin, H. Wang, W. Jiang, A. R. Mkaouar, and P. Xu, "Comparison study on photocatalytic oxidation of pharmaceuticals by TiO_2 -Fe and TiO_2 -reduced graphene oxide nanocomposites immobilized on optical fibers," *Journal of Hazardous Materials*, vol. 333, pp. 162–168, 2017.

[56] M. Crişan, D. Mardare, A. Ianculescu et al., "Iron doped TiO_2 films and their photoactivity in nitrobenzene removal from water," *Applied Surface Science*, vol. 455, pp. 201–215, 2018.

[57] A. J. Haider, R. H. AL–Anbari, G. R. Kadhim, and C. T. Salame, "Exploring potential environmental applications of TiO_2 nanoparticles," *Energy Procedia*, vol. 119, pp. 332–345, 2017.

[58] M. K. Hossain, A. A. Mortuza, S. K. Sen et al., "A comparative study on the influence of pure anatase and Degussa-P25 TiO_2 nanomaterials on the structural and optical properties of dye sensitized solar cell (DSSC) photoanode," *Optik*, vol. 171, pp. 507–516, 2018.

[59] J. Li, D. Ren, Z. Wu et al., "Flame retardant and visible light-activated Fe-doped TiO_2 thin films anchored to wood surfaces for the photocatalytic degradation of gaseous formaldehyde," *Journal of Colloid and Interface Science*, vol. 530, pp. 78–87, 2018.

[60] A. Akbar, A. Payan, M. Fattahi, S. Jor, and B. Kakavandi, "Photocatalytic degradation of rhodamine B and real textile wastewater using Fe-doped TiO_2 anchored on reduced graphene oxide (Fe-TiO_2/rGO): characterization and feasibility , mechanism and pathway studies," *Applied Surface Science*, vol. 462, pp. 549–564, 2018.

[61] J. Shi, G. Chen, G. Zeng et al., "Hydrothermal synthesis of graphene wrapped Fe-doped TiO_2 nanospheres with high photocatalysis performance," *Ceramics International*, vol. 44, no. 7, pp. 7473–7480, 2018.